Journal Name

Dynamic Article Links ►

Cite this: DOI: 10.1039/c0xx00000x

www.rsc.org/xxxxxx

ARTICLE TYPE

$A_x(H_3O)_{2-x}Mn_5(HPO_3)_6$ (A= Li, Na, K and NH_4): Open-Framework Manganese(II) Phosphites Templated by Mixed Cationic Species

Joseba Orive,[a,*] Roberto Fernández de Luis,[b,c] Jesús Rodríguez Fernández,[d] Luis Lezama,[c,e] and María I. Arriortua[b,c]

Received (in XXX, XXX) Xth XXXXXXXXX 20XX, Accepted Xth XXXXXXXXX 20XX

DOI: 10.1039/b000000x

$A_x(H_3O)_{2-x}Mn_5(HPO_3)_6$ (A= Li, x= 0.55 (**1-Li**); A= Na, x= 0.72 (**2-Na**); A= K, x= 0.30 (**3-K**); A= NH_4, x= 0.59 (**4-NH_4**)) phases were synthesized by employing mild hydrothermal conditions. **1-Li** was studied by single crystal X-ray diffraction, while sodium, potassium and ammonium containing analogues were obtained as polycrystalline samples and characterized by powder X-ray diffraction. Four compounds have been characterized by ICP-Q-MS, thermal analyses, and XPS, IR, UV/Vis and EPR spectroscopies. Single crystal data indicate that **1-Li** crystallizes in the P-3c1 space group with lattice parameters a= 10.3764(1) Å and c= 9.4017(1) Å with Z= 2. The crystal structure of these phases is constituted by a three-dimensional $[Mn(II)_5(HPO_3)_6]^{2-}$ anionic skeleton templated by alkali metal and ammonium cations together with protonated water molecules. Such inorganic framework is formed by layers of edge-sharing MnO_6 octahedra placed in the ab plane and joined along the c direction through phosphite pseudotetrahedra. The sheets display 12-membered ring channels parallel to the c-axis, ca. 5 Å in diameter, where the extraframework species revealed a strong disorder. EPR measurements point to the existence of short range ferromagnetic interactions around 12K. Magnetic susceptibility and heat capacity measurements show that all the compounds exhibit long range antiferromagnetic order below circa 4 K, with a significant magnetocaloric effect around the Neel temperature.

Introduction

Metal phosphites are emerging as an interesting family of open framework crystalline materials really attractive in crystal engineering because of their rich structural diversity and derived potential applications in different fields, such as catalysis, photochemistry, adsorption, magnetism and nonlinear optics.[1]

HPO_3 groups can prevent self-interpenetration owing to a fewer number of P-O binding sites, opening the possibilities to construct new porous architectures with large channels that may not be feasible in the classical phosphates family.

For instance, it is remarkable to mention the family of gallium zincophosphites, NTHU-13, with channel sizes ranging from 24-ring to 72-ring. These compounds were successfully achieved by using heterometal centers and a series of aliphatic monoamines increasing from butylamine to octadecylamine.[2]

However, space filling and structure directing effects of the organic molecules normally are responsible for the enhanced stability of the final organic-framework composites. This fact makes really hard to detemplate successfully by calcination while maintaining the microporosity of the inorganic skeleton and as a direct consequence their thermal stability and applicability are reduced.

Another interesting approach to design phosphite type compounds is the use of inorganic template species. The 1+ alkali metal ions can act as templating agents, and moreover, as mobile species once they are incorporated in the crystal framework. Recently some pure inorganic metal phosphites such as $Li_3Fe_2(HPO_3)_3Cl$[3] and $LiFe(HPO_3)_2$[4] have been demonstrated to be electrochemically active for reversible intercalation of Li^+ ions, with an average discharge voltage around 3 V and a practical capacity of about 70 $mAh{\cdot}g^{-1}$. $NaFe_3(HPO_3)_2((H,F)PO_2OH)_6$[5] have also showed excellent capacity retention of Na^+ ions as cathode material for Na-batteries. Furthermore, the assembly of metal phosphite frameworks around hydronium templates has also allowed to obtain inorganic microporous frameworks, such as the nickel and cobalt phosphites, $5H_3O{\cdot}[Ni_8(HPO_3)_9Cl_3]{\cdot}1.5\,H_2O$[6] and $2H_3O{\cdot}[Co_8(HPO_3)_9(CH_3OH)_3]{\cdot}2H_2O$,[7] with extra-large 18-ring channels.

Moreover, the use of three-atom bridges as formate has given rise to the development of materials exhibiting dual property, such as porosity and magnetism.[8] HPO_3^{2-} anion plays the role of three-connector unit which could mimic the formate performance. In this regard, some pure inorganic metal phosphites materials with different magnetic behaviours and porosities have been obtained.[6,7,9]

Inspired by these ideas, here we present a study on an anionic manganese (II) phosphite framework synthesized under mild solution conditions using alkali metal and ammonium cations instead of protonated amines as templates and counterions. $A_x(H_3O)_{2-x}Mn_5(HPO_3)_6$ phases here studied display protonated

water molecules together with the other counteranions highly disordered inside the pores of the structure. Spectroscopic and magnetic properties of $A_x(H_3O)_{2-x}Mn_5(HPO_3)_6$ system will be discussed.

Experimental section

All studied compounds were prepared using mild hydrothermal conditions under autogenous pressure. Lithium compound was obtained as single crystal; however the reaction yield is very low by that synthetic procedure, so other route was designed to obtain good yields as powder samples for all the compounds.

Synthesis of $[Li_{0.55}(H_3O)_{1.45}Mn_5(HPO_3)_6]$ single crystal

A mixture of H_3PO_2 (15.0 mmol) and $MnCl_2.4H_2O$ (1.0 mmol) was dissolved in distilled water (30 ml) and stirred in air. Then, 7.1 mmol of Li_2CO_3 was added to increase up the pH of the resulting solution to 3.5. The reaction mixture was sealed in a 50 ml PTFE-lined stainless steel pressure vessel (fill factor 65%). After 3 days at 170 °C, small transparent prismatic crystals were recovered and washed with water and acetone.

Synthesis of $A_x(H_3O)_{2-x}Mn_5(HPO_3)_6$ (A= Li, Na, K and NH_4) powders and chemical analysis

Compounds $A_x(H_3O)_{2-x}Mn_5(HPO_3)_6$ (A= Li, x= 0.55 (**1-Li**); A= Na, x= 0.72 (**2-Na**); A= K, x= 0.30 (**3-K**); A= NH_4, x= 0.59 (**4-NH_4**)) were synthesized by dissolving a mixture of H_3PO_3 (20 mmol) and $(C_2H_3O_2)Mn{\cdot}2H_2O$ (1 mmol) in 30 ml of H_2O, raising the pH up to approximately 3.3 by adding 18 mmol of the pertinent hydroxide ($LiOH{\cdot}H_2O$, **1-Li**; NaOH, **2-Na**; KOH, **3-K**; NH_4OH, **4-NH_4**). The mixtures placed in the 50 mL Parr Teflon-lined autoclaves were heated for 5 days at 170 ºC, obtaining fine-grained white powders after the reaction.

The metal ion and phosphorous contents were confirmed by inductively coupled plasma quadrupole mass spectrometry (ICP-Q-MS) analysis, performed with a Thermo Scientific XSeries 2 spectrometer. The amount of N in **4-NH_4** was calculated by elemental analysis. $Li_{0.55}(H_3O)_{1.45}Mn_5(HPO_3)_6$ (**1-Li**). Calc: Li, 0.49; Mn, 23.65; P: 34.95. Found: Li, 0.49(1); Mn, 19.6(4); P: 34.4(7). $Na_{0.72}(H_3O)_{1.28}Mn_5(HPO_3)_6$ (**2-Na**). Calc: Na, 2.08; Mn, 23.37; P: 34.54. Found: Na, 2.08(4); Mn, 20.4(4); P: 34.4(7). $K_{0.3}(H_3O)_{1.7}Mn_5(HPO_3)_6$ (**3-K**). Calc: K, 1.46; Mn, 23.27; P: 34.40. Found: K, 1.44(3); Mn, 21.4(4); P: 37.1(7). $(NH_4)_{0.59}(H_3O)_{1.41}Mn_5(HPO_3)_6]$ (**4-NH_4**). Calc: N, 1.04; Mn, 23.46; P: 34.68. Found: N, 1.05(5); Mn, 21.1(4); P: 36.3(7). The densities of the four phases as pressed tablets were measured by flotation[10] using a mixture of diiodomethane and tetrabromoethane, being 3.041(5) $g.cm^{-3}$ for **1-Li**, 2.944(4) $g.cm^{-3}$ for **2-Na,** 3.029(10) $g.cm^{-3}$ for **3-K** and 2.969(2) for **4-NH_4**.

Single crystal X-ray diffraction study

A prismatic single crystal with dimensions 0.100 x 0.071 x 0.038 mm of lithium compound was selected under a polarizing microscope and glued on a glass fibre. Intensity data were collected at 100 K on an Agilent Supernova single source diffractometer with Mo Kα radiation using a CCD (Eos) detector. Data frames were processed (unit cell determination, intensity data integration, correction for Lorentz and polarization effects,[11] and analytical absorption correction[12] taking into account the size and shape of the crystal) using the corresponding diffractometer software package.[13] The structure was solved by direct methods, SHELXS 97 computer program,[14] in the trigonal space group P-3c1, and then refined by the full matrix least-squares procedure based on F^2, using the SHELXL 97 computer program[15] belonging to the WINGX software package.[16]

This procedure allowed us to find the positions of the manganese and phosphorous atoms. Oxygen atoms and the phosphite unit hydrogen were placed from subsequent Fourier-difference map calculations. All non-hydrogen atoms were refined anisotropically.

Three main residual electron densities were observed inside the hexagonal pores which were found to be non-interpretable. Several attempts without success were realized in order to assign the electron densities belonging to these highly disordered extraframework species (See structure refinement in supplementary material, S1).

Since the inorganic building requires two positive charges to achieve electrical neutrality and that the chemical analysis points to the existence of only 0.49% of lithium (0.55 Li atoms per formula), the presence of hydronium cations in the pores is deduced, considering the $Li_{0.55}(H_3O)_{1.45}Mn_5(HPO_3)_6$ formula for compound **1-Li**.

So, the electron densities contribution in the solvent-accessible region to the calculated structure factors in the least-squares refinement of the crystal structure was considered by back-Fourier transformation of them by a SQUEEZE[17] procedure in PLATON.[18] The calculated electron density in the void (39 electrons per unit cell) is close to the deduced content (~35 electrons per unit cell; Z=2, $(H_3O)_{2.9}$ = 31.9e$^-$ and $Li_{1.1}$ = 3.3e$^-$) from the chemical analysis and the electroneutrality requirements. Details of crystal data measurement and reduction, structure solution and refinement of **1-Li** are reported in Table 1.

Table 1 Crystallographic data and structure refinement parameters for **1-Li** obtained by single crystal X-ray diffraction

Molecular weight ($gmol^{-1}$)	785.97
Space group	P-3c1
a, c (Å)	10.3764(1), 9.4017(1)
V ($Å^3$), Z	876.658(15), 2
ρ_{obs}, ρ_{calc} (gcm^{-3})	3.041(5), 2.859
Cristal size (mm)	0.0995 x 0.0706 x 0.0377
F(000)	730
Diffractometer / Temperature (K)	Agilent Supernova (omega scan mode) / 100(2)
μ (mm^{-1}), Tmin./Tmáx.	4.14, 0.774/0.899
Radiation (Å)	λ(Mo Kα) = 0.71073
Limiting indices h, k, l	$-12\leq h\leq 12$, $-12\leq k\leq 11$, $-9\leq l\leq 11$
Theta range (°) Completeness (%)	2.27 - 25.65, 100
N. reflections (measured / independents / observed)	5399 / 562 / 552
R (int) / R(sigma)	0.0227 / 0.0109
Parameters / Restrictions	49 / 0
R [I>2σ(I)]	R1= 0.0502, wR2= 0.1235
R [all data]	R1= 0.0508, wR2= 0.1238
Weight factor	x = 0.0372, y = 17.4760
G. O. F	1.156
Max. and Min. e. density ($eÅ^{-3}$)	3.257, -0.657

Cite this: DOI: 10.1039/c0xx00000x

www.rsc.org/xxxxxx

ARTICLE TYPE

The selected bond distances and angles are reported in ESI, Table S1. Structure drawings were made using the ATOMS 6.2.[19]

Scanning electron microscopy

The microstructures were studied using a JEOL JSM-6400 scanning electron microscope (SEM) equipped with a LaB_6 filament. The measurements were performed using an accelerating voltage of 20 kV and a current intensity around $1 \cdot 10^{-10}$ A, with a working distance of 16 mm. The samples were fixed on double sided carbon tape and coated with a Cr layer (20 nm) deposited by evaporation using a Quorum Q150T Sputter Coater to provide electrical conductivity.

As shown in micrographs in upper insets of Fig. 1(a) prismatic shapes are observed for four compounds $A_x(H_3O)_{2-x}Mn_5(HPO_3)_6$. Particle sizes range from a few hundred nanometers wide to one micron or even some larger crystals up to 2 microns wide as observed in **4-NH$_4$**. They tend to crystallize as very elongated prisms so that its length is highly variable.

Powder X-ray diffraction and XPS characterization

X-ray powder diffraction measurements for qualitative phase analysis using the pattern matching routine of the FULLPROF program[20] for the four compounds were recorded at room temperature using a Philips X'Pert Pro automatic diffractometer equipped with Cu K_α radiation source (λ = 1.5418 Å). The power generator was set to 40 kV and 40 mA and the patterns were recorded in 2θ steps of 0.026° in the 5–70° range. The systematic 2θ shift; peak shape (pseudo-Voigt); *U*, *V*, and *W* half-width parameters for the profile function; the previously obtained unit cell parameters; asymmetry parameters; and the background were refined. Starting from the space group and unit cell parameters of the lithium compound studied by single crystal X-ray diffraction, we reached to good fits for all the compounds synthesized as powder samples with the following unit cell parameters: **1-Li**, a=10.4618(5) Å, c= 9.4057(8) Å, V= 891.5(1) Å^3; **2-Na**, a=10.4881(7) Å, c= 9.3984(10) Å, V= 895.3(1) Å^3; **3-K**, a=10.4380(7) Å, c= 9.4076(10) Å, V= 887.7(1) Å^3; **4-NH$_4$**, a=10.4699(9) Å, c= 9.4350(12) Å, V= 895.7(2) Å^3 (Fig. 1(a) and Table S2). The good agreement between the experimental and the calculated diffractograms confirms the purity of the samples and taking into account the chemical analysis data we have estimated the following formula for the compounds: $Li_{0.55}(H_3O)_{1.45}Mn_5(HPO_3)_6$ (**1-Li**), $Na_{0.72}(H_3O)_{1.28}Mn_5(HPO_3)_6$ (**2-Na**), $K_{0.3}(H_3O)_{1.7}Mn_5(HPO_3)_6$ (**3-K**) and $(NH_4)_{0.59}(H_3O)_{1.41}Mn_5(HPO_3)_6]$ (**4-NH$_4$**). Such cell parameters will be considered later (after structure description section) to discuss the relationships between the size of the unit cells and the pore occupation by the different guest species in $A_x(H_3O)_{2-x}Mn_5(HPO_3)_6$ system.

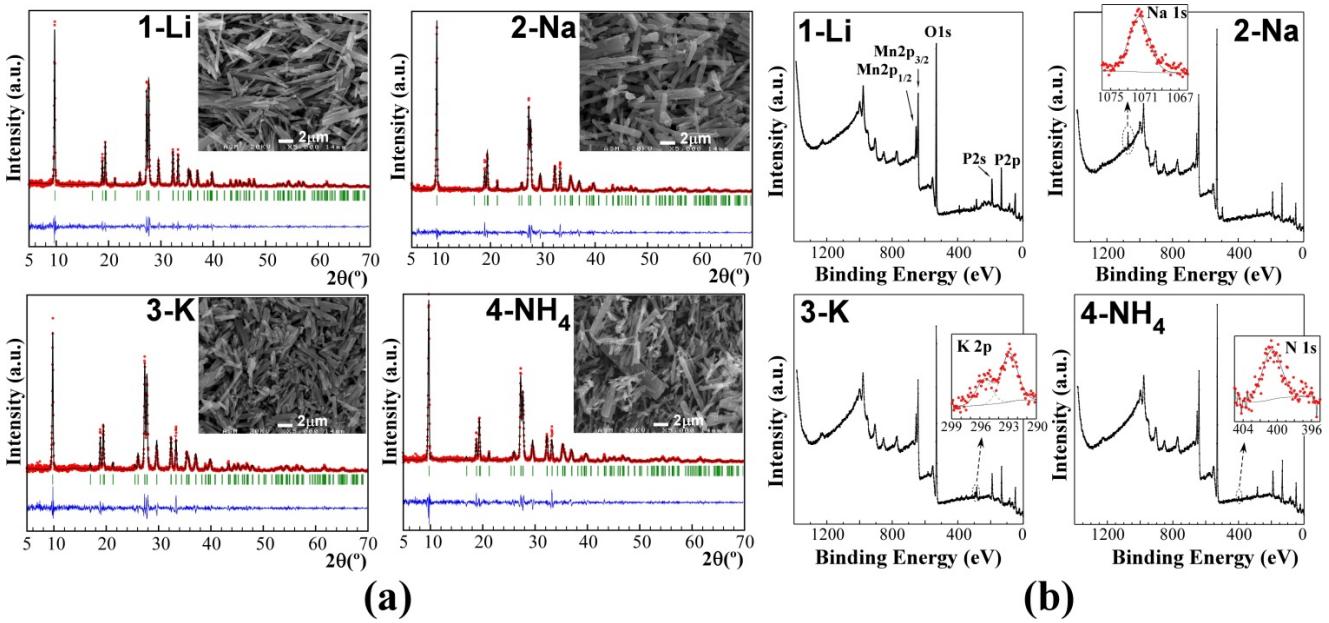

Fig. 1 a) Observed (red dots), calculated (black line) and difference X-ray powder diffraction pattern (blue line) for the pattern matching analysis of **1-Li**, **2-Na**, **3-K** and **4-NH$_4$** compounds. The upper insets show the SEM images of the compounds. b) XPS spectra of the four compounds.

Furthermore, Rietveld refinements were carried out without taking into account the extra-framework species. Some Mn-O and P-O constraints were included to have chemically correct structural models with reasonable bond distances and bond valence data (Tables S2 and S3). The fits are not as good as they could be expected if the positions of the extra-framework species were defined, but they are reliable enough to assure that the crystal framework is the same as one observed by single crystal X-ray diffraction (see Fig. S1).

The chemical composition and the oxidation state of

manganese on the surface of the compounds were assessed by studying the XPS spectra. The fitting together with the binding energies of the P 2p and Mn $2p_{3/2}$ peaks are deposited as Supplementary material (Fig. S2). The insertion of the distinctive cationic species of each compound was easily confirmed by this technique. So that, peaks belonging to Na 1s (1071.7 eV), K 2p (292.9 and 295.6 eV) and N 1s (400.6 eV) were observed in **2-Na**, **3-K** and **4-NH_4**, respectively (Fig. 1(b)). In case of compound **1-Li**, lithium was not possible to detect, in accordance with the sensitivity of the technique for less than 1% of this element, however, its presence was confirmed by ICP-Q-MS.

The Mn 2p core spectrum splits into two peaks due to spin–orbit coupling (Mn $2p_{3/2}$ and Mn $2p_{1/2}$) with a "shake-up" satellite. The decomposition of Mn $2p_{3/2}$ spectra in two main components around 640 and 642 eV suggests the existence of Mn^{2+} in two coordination environments, in agreement with the crystallographic study. Likewise, satellite position from the main Mn 2p emission, centred close to 645.5 eV, also matches the Mn(II) oxidation state behaviour for other manganese phosphate-related compounds.[21] The P 2p peaks are fitted with only one component, according with the unique crystallographic site observed for the phosphorous atom in the structural study. The binding energies around 133 eV are significantly lower than those observed for P(V) species,[22] which is consistent with phosphite groups.[23]

Physicochemical characterization techniques

Thermogravimetric analyses for **1-Li**, **2-Na**, **3-K** and **4-NH_4** were performed under synthetic air on a Netzsch STA 449 F3 Jupiter simultaneous TG-DSC thermo-microbalance. Alumina crucibles containing around 15 mg of every sample were heated in air at a rate of 5 °C/min from room temperature to 800 °C.

Thermodiffractometric experiments for **1-Li** and **2-Na** were carried out in air with a Bruker D8 Advance diffractometer (Cu Kα radiation) equipped with, a variable-temperature stage (HTK2000), a Pt sample heater and a Vantec high-speed one dimensional detector with six degrees of angular aperture. The powder patterns were recorded in the 8≤2θ≤38º range (step size = 0.033º and time per step = 0.4 s) at intervals of 15 ºC, increasing the temperature at 10 ºCmin^{-1} from room temperature to 810 ºC. The IR spectra (KBr pellets) for all compounds were obtained with a Jasco FT/IR-6100 spectrophotometer in the 400-4000 cm^{-1} range. Diffuse reflectance spectra for all compounds were measured at room temperature using a Varian Cary 5000 spectrophotometer in the 200–2500 nm range. X-ray photoelectron spectra of four compounds were acquired using a Specs (Berlin, Germany) system equipped with a Phoibos 150 1D-DLD analyzer, monochromatic AlKα radiation (1486.6 eV, 300 W, 13 kV) and a multi-channel detector. Spectra were recorded in the constant pass energy mode at 80 eV for survey spectra and 30 eV for high resolution spectra, with an electron take-off angle of 90°. The spectrometer was previously calibrated using the Ag 3d5/2 line at 368.26 eV. The binding energy of the adventitious carbon (C1s) was set at 284.6 eV to correct sample charging. The spectra were fitted with the CasaXPS 2.3.16 software, which models the Gauss–Lorentzian contributions, after background subtraction (Shirley). A Bruker Elexsys 500 spectrometer equipped with a super-high-Q resonator ER-4123-SHQ, operating at X band, was used to record the EPR polycrystalline spectrum of **1-Li**. The magnetic field was calibrated by a NMR probe and the frequency inside the cavity was determined with an integrated MW-frequency counter. Magnetic measurements on the powdered samples were performed in the temperature range 2.0-300 K for all compounds, at 0.1 and 0.01 T using a MPMS-7T SQUID magnetometer and a PPMS-system, both from Quantum Design. Heat capacity measurements for **1-Li** and **2-Na** were carried out by a standard two-τ relaxation method, using a PPMS-system, with magnetic fields up to 9 T and temperatures down to 2 K.

Results and discussion

Structure description

The asymmetric unit of the host framework of $Li_{0.55}(H_3O)_{1.45}Mn_5(HPO_3)_6$, **1-Li**, contains two manganese atoms situated in special positions 6f and 4d with .2. and 3.. site symmetries and, one phosphorous, three oxygen and one hydrogen atoms occupying general positions.

The structure of **1-Li** is a three-dimensional network built up by inorganic layers of $Mn(II)O_6$ octahedra joined by HPO_3 pyramids (Fig 2(a)).

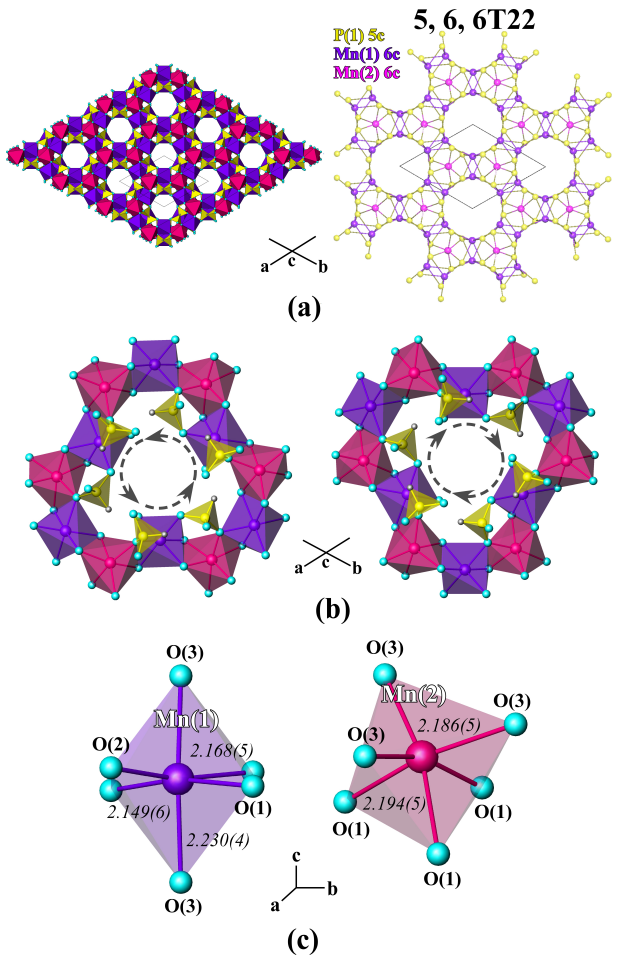

Fig. 2 a) Polyhedral representation and topological view of the 3D crystal structure of **1-Li** viewed along the [001] direction. b) 12- membered ring channels and connectivity with phosphite units. c) Coordination environments of the $Mn(1)O_6$ and $Mn(2)O_6$ octahedra.

Cite this: DOI: 10.1039/c0xx00000x

www.rsc.org/xxxxxx

ARTICLE TYPE

From a topological point of view, the two crystallographically independent manganese atoms are considered as 6-connecting nodes while the phosphorous atom is a 5-connecting one. The simplified underlying net corresponds to a known topology type 5,6,6T22 (Fig. 2(a)). However, this is the first real example of this topology occurring in a crystal structure on the basis of the ToposPro topological collections.[24]

The alternating connection of the $Mn(1)O_6$ and $Mn(2)O_6$ octahedra by edge-sharing gives rise to 12-membered rings (Fig. 2(b)) which extend in the ab plane forming layers. The stacking of these rings in the [001] direction through bridging phosphite groups generates channels 5 Å diameter. Each ring is decorated by six phosphite groups, such that the central phosphorus atom is coordinated to two oxygen atoms of edge-shared octahedra of adjacent layers, and to a third vertex shared with a $Mn(1)O_6$ octahedron. P-H bonds being parallel to the ab-plane arrange clockwise and counterclockwise alternately in the stacking direction of the layers (Fig. 2(b)).

In the $[Mn(1)O_6]$ and $[Mn(2)O_6]$ polyhedra the Mn-O bond lengths range from 2.149(6) to 2.230(4) Å and from 2.186(5) to 2.194(5) respectively (Fig. 2(c)) in good agreement with 2+ oxidation state for both manganese atoms, based on the bond valence sums (BVS) calculations.[25] *Cis* angles vary from 78.5(2)º to 99.1(2)º and from 79.0(2)º to 103.4(1)º for Mn(1) and Mn(2) respectively. *Trans* angles values are in the 168.1(2)º-176.8(3)º range in $[Mn(1)O_6]$, being 162.7(2)º in $[Mn(2)O_6]$. The $S(O_h)$ values, calculated by Continuous Symmetry Measure,[26] are 0.953 and 1.526 for $Mn(1)O_6$ and $Mn(2)O_6$ octahedra respectively, near the value for the octahedral ideal symmetry (S(Oh) = 0.00).

The P-O distances of the $(HPO_3)^{2-}$ unit are in the range 1.528(5)-1.540(6) Å and the P-H distance is 1.26(7) Å. The O-P-O angles vary from 107(3)º to 114.1(3)º and the H-P-O angle is 105(3)º which are in the usual range for phosphite based compounds.[27]

As we mentioned in the single-crystal X-ray diffraction study, the extraframework species occupying the pores could not be crystallographically defined. However, chemical analysis allowed us to define the amount of lithium present in the channels and consequently the amount of hydronium cations necessary to offset the negative charge excess of the inorganic building of **1-Li**.

Structure discussion

The host framework of **1-Li** is isotypic to the mixed valent Fe^{II}/Fe^{III} phases $Li_{1.43}[Fe^{II}_{4.43}Fe^{III}_{0.57}(HPO_3)_6]\cdot 1.5H_2O$[28] and $K_{0.75}[Fe^{II}_{3.75}Fe^{III}_{1.25}(HPO_3)_6]\cdot 0.5H_2O$[29] and the iron(II) dehydrated phase $(NH_4)_2[Fe^{II}_5(HPO_3)_6]$.[30] In all of them, cationic species inside the pores compensate the anionic charge of the framework, being unnecessary the protonation of crystallization water molecules. The Mn-O distance ranges (Mn(1)-O = 2.149(6)-2.230(4) Å and Mn(2)-O = 2.186(5)-2.194(5) Å) are quite different from the Fe-O distances observed in the iron phases, where Fe(1)-O = 2.032(2)-2.186(2) Å, 2.046(2)-2.179(2) Å and 2.030(3)-2.217(3) Å and Fe(2)-O = 2.134(1)-2.141(2), 2.134(2)-2.143(2) Å and 2.138(3)-2.140(3) Å for $Li_{1.43}[Fe^{II}_{4.43}Fe^{III}_{0.57}(HPO_3)_6\cdot 1.5H_2O$,[28] $K_{0.75}[Fe^{II}_{3.75}Fe^{III}_{1.25}(HPO_3)_6]\cdot 0.5H_2O$[29] and $(NH_4)_2[Fe^{II}_5(HPO_3)_6]$[30] compounds respectively. Such metal-oxygen bond lengths differences cause a marked increase of the unit cell parameter *c* of the manganese phases with regard to iron phases as can be observed in the values represented in Fig. 3. This fact could be closely correlated with the differences observed in the extra-framework content of them.

For the specific case of the studied compounds three variables are involved in the structural behaviour of the unit cell; i) the ionic radii of the A cations, ii) the occupation factor of the A cations, and iii) the A/H_3O^+ packing efficiency within the pores.

It is difficult to reach a meaningful conclusion regarding the effect of such variables in the cell parameters of the crystal structure only with the data obtained from the manganese compounds. For sake of comparison we have also analysed the effect of the A cations in the cell parameters of the previously mentioned isomorphous iron-bearing compounds of $A_{2-x}[Fe^{II}_{5-x}Fe^{III}_x(HPO_3)_6]\cdot nH_2O$ formula. Fig. 3 shows the unit cell parameters versus the A site occupation degree plots for $A_x(H_3O)_{2-x}Mn_5(HPO_3)_6$ and $A_{2-x}[Fe^{II}_{5-x}Fe^{III}_x(HPO_3)_6]\cdot nH_2O$ systems. The unit cell parameter values for $A_x(H_3O)_{2-x}Mn_5(HPO_3)_6$ system were obtained from the pattern matching analyses of the powder X-ray diffractograms and those ones for iron compounds were obtained from their respective single-crystal X-ray diffraction studies.

It seems that the main factor affecting the crystal parameters is the occupation factor of the A cations, giving rise to a linear increase of the "*a*" parameter with the increase of the A site occupation, which involves an opening of the one dimensional channel. The deviations from the linearity of the "*c*" parameter evolution, and concretely for the ammonium-containing compound, could be ascribed to a less packing efficiency between the NH_4^+ and H_3O^+ cations within the pores. But clearly, and in the same direction observed for the $A_{2-x}[Fe^{II}_{5-x}Fe^{III}_x(HPO_3)_6]\cdot nH_2O$ family, the occupation factor of A cations effect governs the aperture dynamic of the one-dimensional channels. Ionic radii of the alkali metal and ammonium ions also influence the reorganization of the crystal structure but its effect is partially covered up by the occupation degree of such species (see Fig. S3).

Cite this: DOI: 10.1039/c0xx00000x

www.rsc.org/xxxxxx

ARTICLE TYPE

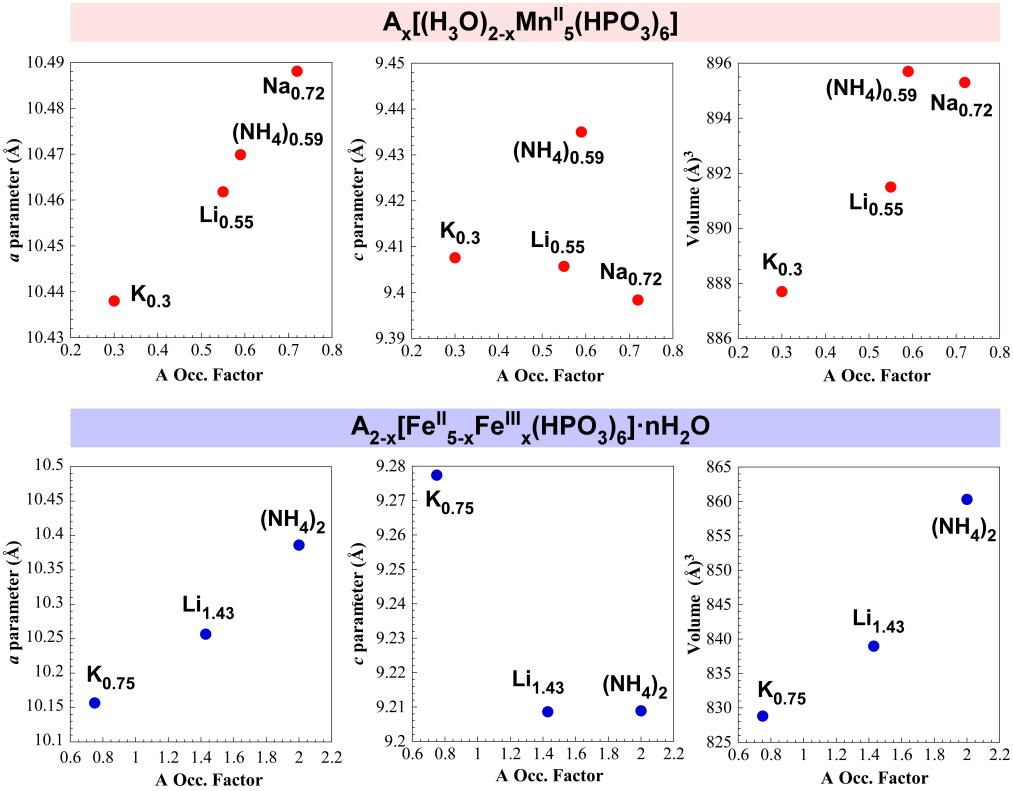

Fig. 3 Comparison of unit cell parameters versus A site occupation degree in $A_x(H_3O)_{2-x}Mn_5(HPO_3)_6$ system (compounds here studied, **1-Li**, **2-Na**, **3-K** and **4-NH$_4$**) and isotypic iron compounds $A_{2-x}[Fe^{II}_{5-x}Fe^{III}_x(HPO_3)_6]\cdot nH_2O$ previously reported.[28-30] Subscripts refer to the atoms per unit formula of A species.

Thermal study

The thermal stability of the samples was studied by means of thermogravimetry and thermodiffractometry. For the thermogravimetric experiments, firstly, the behaviour of the lithium sample will be explained, so that a comparison with the thermal decomposition of the sodium, potassium and ammonium compounds will be established later. For **1-Li** two thermogravimetric experiments were carried out, the first one with the as-synthesized sample, and the second one after one month of exposition to ambient conditions (Fig. S4(a)). The TG curve for the **1-Li** as-synthesized sample shows three different weight changes: for the first one, from 250ºC to 385ºC, 1.57 % of weight loss is attributed to the release of hydronium cations from the crystal structure. The observed weight loss (1.57 %) is far from the theoretical one expected for the release of 1.45 H_3O^+ per formula unit (3.51 %). Above 385ºC, and up to 500ºC, the TG curve can be explained based on the competition between the weight loss ascribed to the release of hydronium cations and the beginning of the oxidation of the phosphite groups. The weight gain due to the P(III) to P(V) oxidation during the decomposition masks the weight loss of the hydronium cations, and hence, the observed weight loss of hydronium cations (1.57%) is smaller than the theoretical one (3.51%). The third step in the thermal decomposition of **1-Li** is observed above 500ºC. After the complete release of hydronium cations, a weight gain is exclusively observed and ascribed to the complete oxidation of the phosphite groups and the formation of the inorganic residues. The main difference between the thermogravimetric curve of the as-synthesized compound and the sample exposed one month to ambient conditions is observed between 30 and 135ºC and related to the loss of adsorbed water molecules. It is difficult to assure if the water molecules are surface adsorbed or are incorporated within the pores of the crystal structure, but the hydrophilic character of the compound is clear.

For **2-Na**, **3-K** and **4-NH$_4$** similar thermal decomposition of the samples is observed (Fig. S4(b)). The lithium and potassium thermogravimetric curves are very similar. For **4-NH$_4$**, the loss of ammonium and hydronium cations seems to be less overlapped with the phosphite groups oxidation than in the other samples, and hence a higher weight loss value is observed in the first stage of the thermal analysis. Regarding **2-Na**, the first weight loss observed in the 30-135ºC temperature range is ascribed to adsorbed water molecules. Such behaviour was previously described for the lithium sample exposed to ambient conditions.

In DSC curves exothermic peaks at 554ºC for **1-Li** and **2-Na**, 570ºC for **3-K** and 580ºC for **4-NH$_4$** are observed, being less

intense those that appear at higher temperatures. Such effect could be correlated with the crystallinity grade of the inorganic residue as can be seen in the diffraction patterns of them after heat treatment (Fig. S.4(c)). DSC curve of **4-NH_4** also shows two broad exothermic peaks with low intensity at 650ºC (with a mass gain of 1.25%) and 740ºC. At this last temperature, DSC curve of **2-Na** shows a sharp exothermic peak associated with a mass increase of around 1.7% related to the crystallization of an inorganic residue. A main common calcination product composed by a monoclinic $Mn_2P_2O_7$ (*PDF file:* 01-072-2043; S.G. C2/m (12), a= 6.630 Å, b= 8.580 Å, c= 4.540 Å, β= 102.66º) with some other less intense peaks of unidentified phases for the four compounds is observed (Fig. S.4(c)).

The thermodiffractometry in air of **1-Li** and **2-Na** show that the diffraction maxima of the phases remain unchanged until 270 ºC. Since this temperature diffraction peaks begin to decrease in intensity, disappearing practically at 330 ºC, temperature at which compounds become amorphous as a result of the hydronium cations release (Fig. S.5). Cell parameter evolution was studied with increasing temperature by cyclic pattern matching refinements of the X-ray patterns (Fig. S.6). *c* parameter remains practically constant until 200ºC, decreasing slightly from this temperature to the destruction of crystalline structures of both compounds. *a* parameter and unit cell volume of **2-Na** exhibit a constant increase with thermal expansion coefficients of around $18 \cdot 10^{-6}$ and $34.5 \cdot 10^{-6}$ $ºC^{-1}$, respectively in the 30-270 ºC temperature range. Meanwhile both parameters in **1-Li**, stop growing in the 120-225 ºC temperature range, possibly due to small reorientation movements of the structural units before hydronium cations release.

Infrared and UV-Vis spectroscopy

In the infrared spectra of the four compounds (Fig. S.7)**,** the presence of the $(HPO_3)^{2-}$ groups is confirmed by the existence of a medium intensity narrow band situated at 2485 cm^{-1} corresponding to the stretching vibrational mode of the P-H bond. At lower frequencies, in the 1200-400 cm^{-1} the rest of the bands corresponding to the P-O bonds vibrations of the phosphite groups are observed. The spectra exhibit a very broad absorption between 3000 and 3500 cm^{-1} for the O-H stretching vibration. The stretching (~3190 cm^{-1}) and deformation (~1455 cm^{-1}) modes attributed to the triply degenerate vibrations of the NH_4^+ ion[31] are observed in the spectrum of **4-NH_4**, whose values are very similar to those ones found in $(NH_4)_2[Fe^{II}_5(HPO_3)_6]$.[30]

The d–d absorption transitions of Mn^{2+} ion in four compounds are strongly forbidden, in such a way that only a very low intensity band can be observed at 407 nm, which has been assigned to a transition from $^6A_1(^6S)$ ground state to $^4E(^4G)$ term (Fig. S.8(a)), according to the white colour exhibited by the phases. Fig. S8(b) shows the diffuse reflectance spectra of four compounds. Absorption (K/S) data were calculated from the following Kubelka-Munk function:[32]

$$F(R) = (1 - R)^2/2R = K/S$$

with *R* representing the reflectance, *K* the absorption, and *S* the scattering. In a *K/S* vs *E* (eV) plot, extrapolating the linear part of the rising curve to zero provides the onset of absorption. The values of energy band gaps vary slightly depending on the alkali metal ions content being 2.66 eV for **3-K**, 2.75 eV for **4-NH_4** and 2.82 eV for **1-Li** and **2-Na**.

EPR spectroscopy

X-band EPR spectrum of **1-Li** was performed for a powdered sample at room temperature and exhibits an isotropic centered signal due to the presence of high-spin coupled Mn(II) cations (Fig. S9(a)). The EPR signal was fitted by Lorentzian curves with the *g* gyromagnetic factor being 2.011(2), which remains practically unchanged when the sample is cooled down to 10 K and increases slightly at lower temperatures (g=2.023 at 5 K).

The simplified thermal variation of the spectra from room temperature to 4K is shown in Fig. 4(a) (See Fig. S9(b) for all the temperatures recorded). A continuous increase of the intensity from 280K to approximately 50 K can be observed, in good agreement with a paramagnetic state of the manganese ions (Fig. 4(b)). Below this temperature the signals abruptly broaden and gain intensity, according to a more effective spin correlation resulting from the exchange interactions. Moreover, an increase in the slope of the Intensity vs T and Line-width vs T curves can be observed at 12 K, probably related to the presence of short range magnetic order of ferromagnetic nature as we will discuss later.

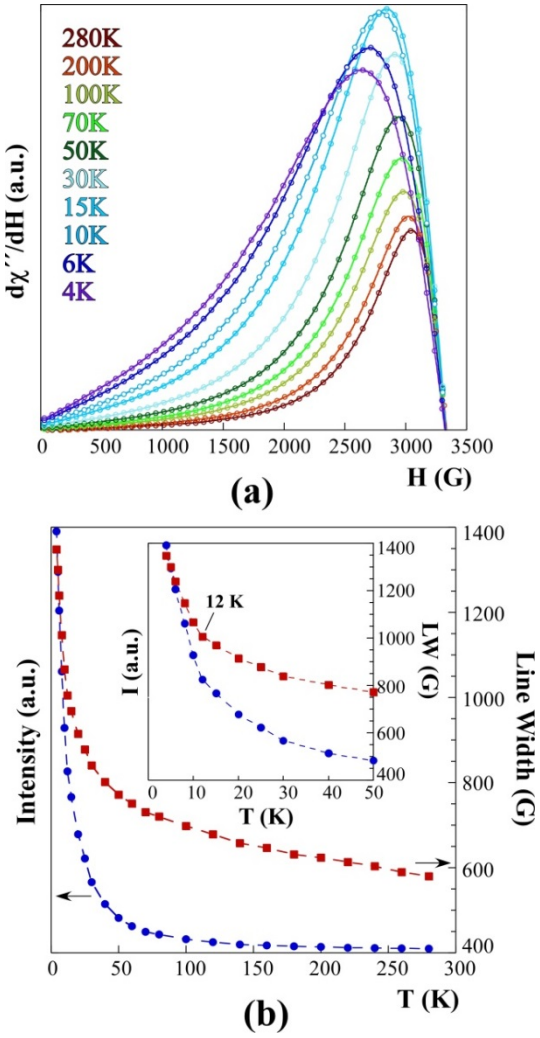

Fig. 4 a) X-band powdered EPR spectra at different temperatures for **1-Li**. b) Thermal evolution of the line-width and intensity of the EPR signals of **1-Li**.

Magnetic behaviour

Variable temperature magnetic susceptibility measurements of **1-Li**, **2-Na**, **3-K** and **4-NH$_4$** compounds were carried out in the 2-300 K temperature range under a magnetic field of 1 kOe. The molar magnetic susceptibility of **1-Li** increases as the temperature decreases and reaches a smoothly rounded maximum at approximately 4 K (Fig. 5). This feature is better observed in the derivative of the susceptibility ($d\chi_m/dT$), where a clear maximum appears (see upper inset of Fig. 5) defining a magnetic transition temperature of 4.2 K. Above this temperature χ_m follows the classical Curie−Weiss law, in fact, $1/\chi_m$ has a perfect linear behaviour, enabling the calculation of a Weiss temperature and the average effective paramagnetic moment per Mn ion (θ_p = -15.39 K and μ_{eff} = 6.08 μ_B)**.** The general behaviour of the other compounds is very similar, see Fig. S10, being the obtained fitted parameters θ_p = -14.26 K and μ_{eff} = 6.02 for **2-Na**, θ_p = -16.43 K and μ_{eff} = 6.10 for **3-K** and θ_p = -17.67 K and μ_{eff} = 6.12 for **4-NH$_4$**. The value of μ_{eff} for all the compounds is very close to the theoretical one (μ_{eff} = 5.92 μ_B) obtained from $\mu_{eff} = g[S(S + 1)]^{1/2}$, considering high-spin S = 5/2 Mn^{2+} cations with no orbital contribution. The negative θ_p value, together with the reduction of the effective magnetic moment (χ_mT) observed when the temperature is decreasing (not shown) suggests global antiferromagnetic interactions in all compounds.

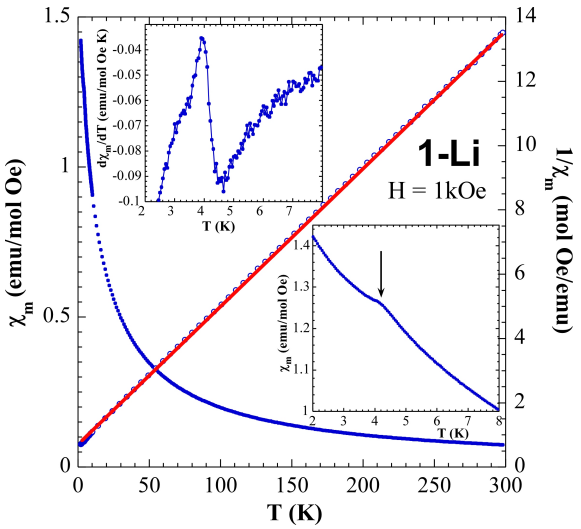

Fig. 5 Temperature dependence of the molar susceptibility (χ_m) and $1/\chi_m$ measured at 1 kOe for **1-Li**. The solid red line is the fit according to Curie–Weiss law. The insets show an enlargement of the low temperature region, in the lower the susceptibility (χ_m) and in the upper the derivative of the susceptibility ($d\chi_m/dT$).

The results of the low temperature magnetic susceptibility measured warming under 1 kOe after cooling down from room temperature first without an applied field [zero field cooled (ZFC)] and subsequently under applied field [field cooled (FC)], are shown in Fig. 6. All the compounds exhibit a rounded maximum, which define Neel temperatures (marked with arrows in Fig. 6) of 4.2 K for **1-Li** and **3-K**, 4.0 K for **4-NH4** and 3.2 K for 2-Na. In addition the curves do not show any irreversibility, indicating the absence of any ferromagnetic component.

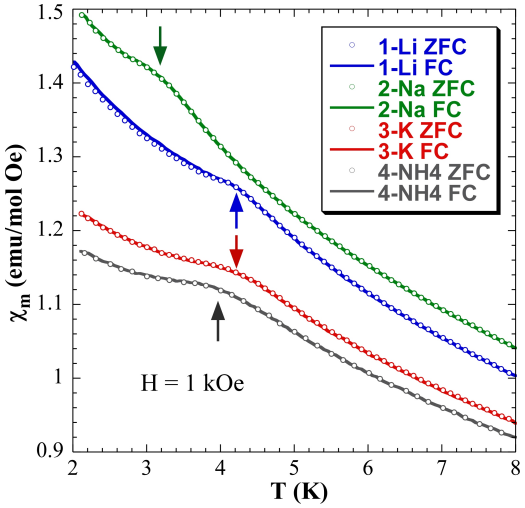

Fig. 6 Low field ZFC–FC magnetic susceptibility of the four studied compounds taken at an applied field of 1 kOe. The arrows show the Neel temperatures.

Fig. 7 depicts the magnetization as a function of the magnetic field at T = 2 K compared for the four studied compounds. The magnetization shows no hysteresis at this temperature, in the ordered state, thereby excluding the existence of any ferromagnetic component, in good agreement with the ZFC-FC data. Moreover, the magnetization rises continuously, and does not show saturation up to 90 kOe. In fact, the magnetization values attained in this magnetic field, comprised between μ = 3.06 μ_B/Mn for **4-NH$_4$** and μ = 3.51 μ_B/Mn for **2-Na**, are far from the expected fully-saturated value of 5 μ_B of the Mn^{2+} cation. Similar reduction was observed in the Sarkinite phase, $Mn_2(OH)AsO_4$, and was attributed to the existence of a strong magnetocrystalline anisotropy.[33]

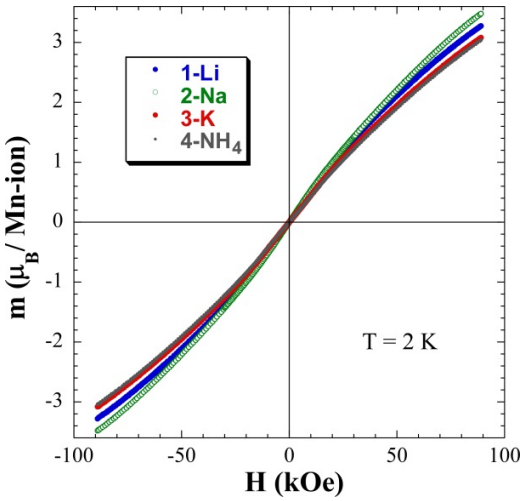

Fig. 7 Magnetization vs. applied magnetic field at 2 K for the four studied compounds.

Fig. 8 shows the temperature dependence of the molar heat capacity (C_P) of **1-Li** and **2-Na** compounds, between 2 and 300 K. In the absence of an external magnetic field, C_P reveals a sharp maximum at 4 and 3 K for **1-Li** and **2-Na**, respectively (see lower insets in Fig. 8). This anomaly reveals a second-order transition and it can be related to the establishment of three-dimensional

antiferromagnetic order in agreement with the magnetic-susceptibility data. The continuous growth of Cp at higher temperatures is due to the lattice contribution (C_{pho}), which does not show any tendency to saturation. In fact, the Cp values at 300 K for both compounds are around 600 J/molK, still far from the expected values (**1-Li**, 1031.4 and **2-Na**, 1000.7 J/molK) according to the Dulong and Petit law for the 41.35 and 40.12 ions per unit formula for **1-Li** and **2-Na**, respectively. This is due to the presence of light atoms with very high excitation energy.

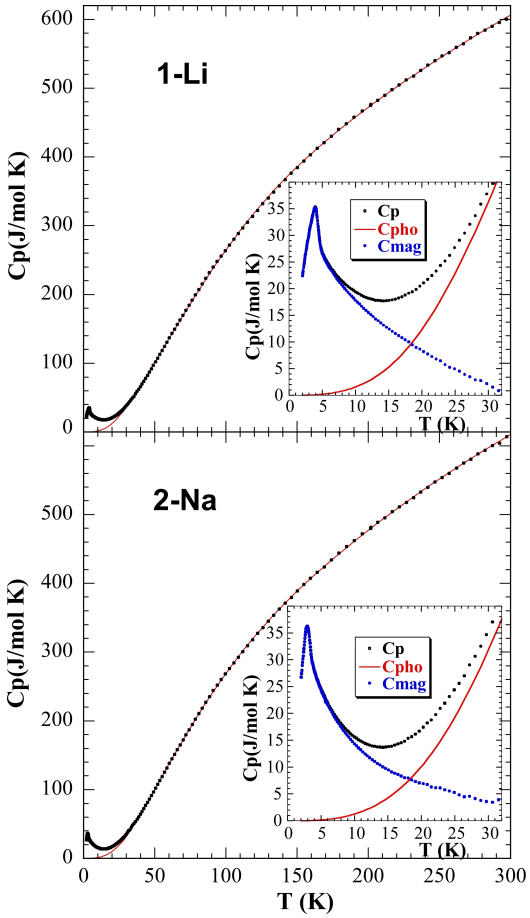

Fig. 8 Specific heat of **1-Li** and **2-Na** compounds between 2 and 300 K. The black full dots are the experimental data and the red dashed line the estimated phonon contribution. Lower inset shows an enlargement of the low temperature region including the magnetic contribution (blue full dots).

In order to extract the magnetic contribution, C_{mag}, the C_{pho} was estimated using the Debye model and considering the existence of three Debye temperatures (the minimum number of free parameters that will allow us to fit the experimental data). In this way, if the number of atoms in the unit cell is N, we suppose n_1 atoms with a Debye temperature θ_{D1}, n_2 atoms with a Debye temperature θ_{D2}, and n_3= (N-n_1-n_2) atoms with a Debye temperature θ_{D3}. Therefore, there are five free parameters, namely, n_1, n_2, θ_{D1}, θ_{D2}, and θ_{D3}. This approach has been used successfully in previous studies in other hybrid compounds.[34] The best fittings are obtained for n_1 = 6.1, θ_{D1}= 206 K, n_2 = 15.2, θ_{D2}= 513 K and θ_{D3}= 1832 K for compound **1-Li** (N = 41.3) and n_1 = 8.4, θ_{D1}= 246 K, n_2 = 12.4, θ_{D2}= 531 K and θ_{D3}= 1669 K for compound **2-Na** (N = 40.1). The good quality of the fits (see the continuous lines in Fig. 8) allows us to consider that this phenomenological model determines reasonably well the phonon contribution. The magnetic contributions, obtained as C_{mag} = Cp − C_{pho}, are plotted in the insets of Fig. 8 for compounds **1-Li** and **2-Na**. The long tail at temperatures above the maximum could be associated with the persistence above T_C of pronounced short-range order as observed in the EPR measurements. The values of Cp_{mag} in the maximum are very similar for both compounds, being 35.2 J/mol K for **1-Li**, and 36.2 J/mol K for **2-Na**. This means that the jump of C_{mag} at T_C per magnetic ion (ΔC_{mag}/Mn ≈ 0.85R, is much lower than the expected one for equal moment (EM) magnetic structures, C_{mag}^{EM} =2.36R for S= 5/2 within the molecular field approximation.[35,36] This reduction, together with the small signal in the susceptibility at the Neel temperature, points toward a complex magnetic structure, probably of incommensurate type.

Heat-capacity has been also studied in the presence of several magnetic fields. Because the phonon contribution is not affected by the magnetic field, we have subtracted those values from the experimental data and obtained the magnetic contributions (see Fig. 9). With increasing field, the sharp λ-type magnetic peak becomes more rounded and shifts to lower temperatures, as can be better observed in the inset of Fig. 9.

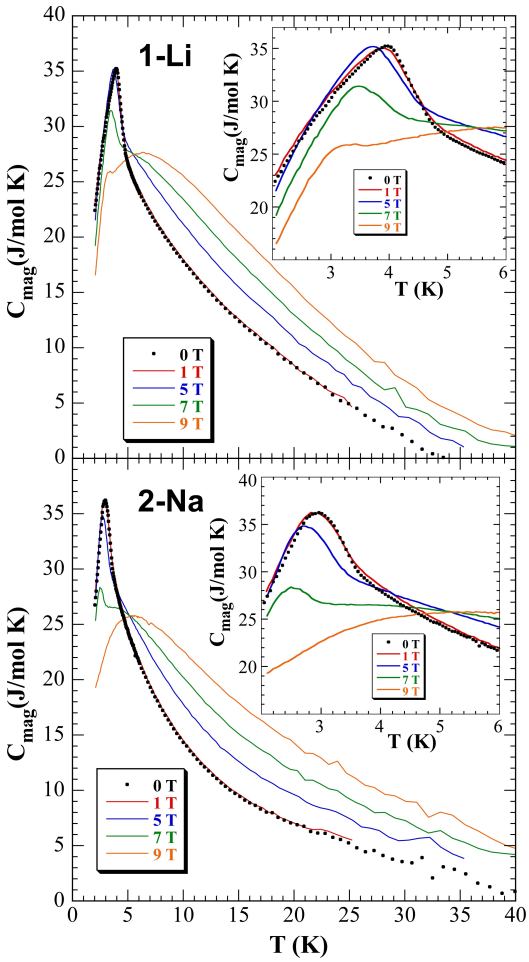

Fig. 9 Temperature dependence of the magnetic specific heat (C_{mag}) of **1-Li** and **2-Na** compounds under different magnetic fields. The inset shows an enlargement around the peak.

This behaviour clearly proves the antiferromagnetic character of the magnetic transition.[35] We should notice that in the case of ferromagnetic transitions, the peak shifts to higher temperatures.[37] In addition, the increase of C_{mag} above T_N with field is a common effect, associated to the fact that the magnetic field favors the short range ferromagnetic correlations.

The magnetic entropy variation,

$$S = \int (C_{mag}/T) dT,$$

is plotted in Fig. S11 for **1-Li** and **2-Na**. The maximum entropy value, being reached around 30 K, was found to be 70 J/molK for both compounds. This result is in agreement with the theoretical value, 74.2, expected for a system with 5 magnetic ions with a *S*=5/2 spin state.

The strong field dependence of C_P must give rise to the appearance of an important magnetocaloric effect (MCE) at low temperatures. In order to calculate the MCE, we determined the total entropy,

$$S = \int (C_p/T) dT,$$

and then used the method described in Ref. [38]. The isothermal magnetic entropy change (-ΔSm) and the adiabatic temperature change (ΔT_{ad}) are depicted in Fig. 10 for **1-Li** and **2-Na.** In both compounds -ΔSm exhibit a peak centred at the Neel temperature, which is better defined as the magnetic field increases, arriving to a maximum value at 9T of ΔS_m^{max} = 16.1 and 17.2 J/kg·K for **1-Li** and **2-Na** respectively. The adiabatic temperature change exhibits a wider peak centred at around 11 K, with maximum values at 9 T of ΔT_{ad}^{max} = 4.2 and 5.5 K for **1-Li** and **2-Na** respectively. Although these values are lower than those obtained in the low temperature range in some molecular magnets,[39] the magnetocaloric effect is relatively important. In fact, the values of ΔS_m^{max} and ΔT_{ad}^{max} are similar,[40] or even larger[41] than those found in other antiferromagnetic materials with close Neel temperatures.

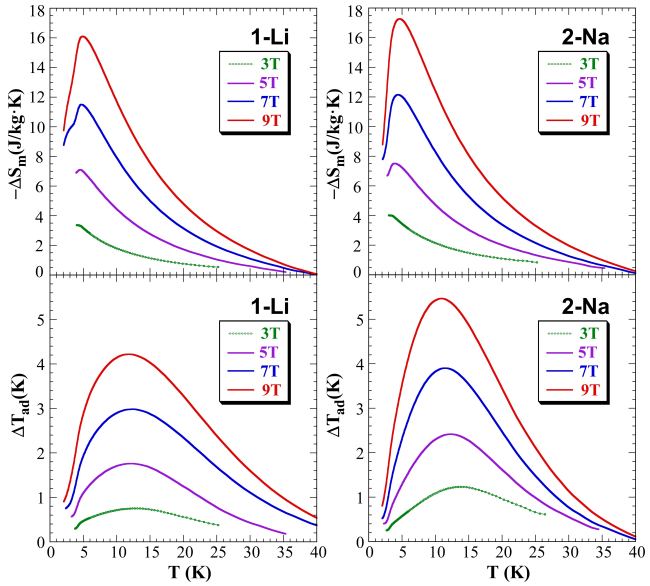

Fig. 10 Temperature dependence of the isothermal magnetic entropy change (-ΔS_m) and the adiabatic temperature change (ΔT_{ad}) at various applied magnetic fields for **1-Li** and **2-Na** determined from heat-capacity measurements.

Taking into account the crystal structure of **1-Li**, mainly intra-layer magnetic pathways are deduced (Fig. S12). Metal-metal distance is 3.34 Å so that direct interactions probably are not feasible, but these are represented by intradimeric interactions via edge-sharing oxygen atoms between the $Mn(1)O_6$ and $Mn(2)O_6$ octahedra, whose exchange angles are 98.42º and 100.09º. Finally, $|HPO_3|$ pyramids ensure the further 3D crystal linkage, giving rise to the superexchange interlayer Mn–O–P–O–Mn interactions as observed in the magnetic susceptibility and heat capacity measurements.

As in $A_x(H_3O)_{2-x}Mn_5(HPO_3)_6$ system, magnetic susceptibility of the isostructural phase $Li_{1.43}[Fe^{II}_{4.43}Fe^{III}_{0.57}(HPO_3)_6 \cdot 1.5H_2O$ showed a peak at low temperature, in this case at 6K.[28] This maximum could be attributed to antiferromagnetic interactions. Nevertheless, the existence of clear irreversibility below this temperature concurs with a spin-glass state. The existence of random mixed valence iron cations enhances the spin frustrations, and the occurrence of both, randomness and frustration, explains this particular magnetism.

In our system, Mn-O-Mn exchange angles around 100º can generate interactions at the border between the F and AF characters, leading to frustration as demonstrated by the small signals observed in the susceptibility and the heat capacity measurements. However, all the manganese atoms have the same magnetic moment, suppressing the randomness of the magnetic interactions and the consequent spin glass behaviour[42] observed in the mixed-valent iron analogue.

Conclusions

Four new manganese (II) phosphites templated by alkali metal ions (Li^+, Na^+ and K^+) and ammonium cations were achieved under mild hydrothermal conditions. The skeleton of **1-Li**, solved by single crystal X-ray diffraction, is constituted by layers of edge-shared $Mn(II)O_6$ octahedra linked along the [001] direction through phosphite units. Manganese octahedra form 12-membered ring channels parallel to the stacking direction, ca. 5 Å in diameter, where the templating species (A site) are highly disordered together with H_3O^+ cations. The A site occupation effect is crucial in the pore opening degree, even more than the ionic radius of the guest species themselves. Moreover, the stacking of the inorganic layers along the [001] direction is probably affected by the A/H_3O^+ packing efficiency within the pores.

According to the EPR measurements and the Cp behaviour above T_C, 2D short-range ferromagnetic interactions within the inorganic layers seem to be established around 12K. Such magnetic order could be the precursor for the global three-dimensional antiferromagnetic behaviour of all the phases below around 4K as observed in the magnetic susceptibility and heat capacity measurements. Intralayer pathways characteristics could frustrate the magnetic exchange system, giving rise to a complex magnetic behaviour probably related to an incommensurate magnetic structure. However, comparing with $Li_{1.43}[Fe^{II}_{4.43}Fe^{III}_{0.57}(HPO_3)_6 \cdot 1.5H_2O$,[28] it seems that the nature and the unique oxidation state, +2, of the manganese atoms in $A_x(H_3O)_{2-x}Mn_5(HPO_3)_6$ suppresses the randomness in the magnetic interactions observed in the isostructural compound, eliminating the spin-glass state. Finally, the compounds exhibit

an important magnetocaloric effect at low temperatures.

Acknowledgments

This work has been financially supported by the "Ministerio de Economía y Competitividad" (MAT2013-42092-R and MAT2014-55049-C2-R) and the "Gobierno Vasco" (IT630-13) and the "UPV/EHU" (UFI11/15), which we gratefully acknowledge. The authors thank the technicians of SGIker (UPV/EHU) financed by the National Program for the Promotion of Human Resources within the National Plan of Scientific Research, Development and Innovation, "Ministerio de Ciencia y Educación" and "Fondo Social Europeo" (FSE), for technical and human support. Joseba Orive wishes to thank CONICYT for the 2015 FONDECYT postdoctoral project (Nº 3150455).

Notes and references

[a] *Departamento de Ciencia de los Materiales, FCFM, Universidad de Chile, Av. Beauchef 851, Santiago 8370448, Chile. Fax: +56 2269 94119; Tel: +56 2297 71076; E-mail: joseba.orive@ing.uchile.cl.*
[b] *Departamento de Mineralogía y Petrología, Facultad de Ciencia y Tecnología, Universidad del País Vasco (UPV/EHU), Apdo. 48940 Leioa, Spain. Fax: +34 946 013 500; Tel: +34 946 015 984; E-mail: roberto.fernandez@ehu.eus, maribel.arriortua@ehu.es.*
[c] *Basque Center for Materials, Applications & Nanostructures (BC Materials) Parque Tecnológico de Zamudio, Camino de Ibaizabal, Edificio 500 - 1º, 48160 Derio, Spain. Tel: +34 946 128 811; E-mail: roberto.fernandez@bcmaterials.net, maribel.arriortua@ehu.es.*
[d] *CITIMAC, Facultad de Ciencias, Universidad de Cantabria, 39005 Santander, Spain. Fax: +34 942 201 402; Tel: +34 942 201 511; E-mail: rodrigufj@unican.es.*
[e] *Departamento de Química Inorgánica, Facultad de Ciencia y Tecnología, Universidad del País Vasco (UPV/EHU), Apdo. 48940 Leioa, Spain. Fax: +34 946 013 500; Tel: +34 946 012 703; E-mail: luis.lezama@ehu.es.*

† Electronic Supplementary Information (ESI) available: structure refinement information, bond distances and angles for 1-Li, Rietveld analysis, XPS spectra, unit cell parameters vs ionic radius, thermal analyses, infrared spectra, UV-Vis spectra, EPR spectra for 1-Li, thermal evolution of molar susceptibility for 2-Na, 3-K and 4-NH_4, thermal dependence of the magnetic entropy of 1-Li and 2-Na and magnetic exchange pathways for 1-Li. CCDC 1469966. See DOI: 10.1039/b000000x/

1 J. Orive, E. S. Larrea, R. Fernández de Luis, M. Iglesias, J. L. Mesa, T. Rojo, M. I. Arriortua, *Dalton Trans.*, 2013, **42**, 4500; C-M. Wang, T-Y. Chang, C-W. Chiu, H-M. Lin, K-H. Lii, *Inorg. Chem.*, 2014, **53**, 3266; T. Rojo, J. L. Mesa, J. Lago, B. Bazán, J. L. Pizarro, M. I. Arriortua, *J. Mater. Chem.*, 2009, **19**, 3793; J-L. Song, J-H. Zhang, J-G. Mao, *J. Solid State Chem.*, 2016, **237**, 371; L. Xianchun, X. Yan, W. Xinlong, X. Hongbin, L. Xizheng, S. Kuizhan, S. Zhongmin, *Chem. Comm.*, 2010, **46(15)**, 2614; H-L. Huang, Y-C. Lai, Y-W. Chiang, S-L. Wang, *Inorg. Chem.*, 2012, **51(4)**, 1986; J-L. Song, C-L. Hu, X. Xu, F. Kong, J-G. Mao, *J. Solid State Chem.*, 2015, **231**, 198; J. Zhang, Z. Yao, S. Liao, J. Dai, Z. Fu, *J. Mater. Chem. A,* 2013, **1**, 4945.

2 H-Y. Lin, C-Y. Chin, H-L. Huang, W-Y. Huang, M-J. Sie, L-H. Huang, Y-H. Lee, C-H. Lin, K-H. Lii, X. Bu, S.-L. Wang, *Science*, 2013, **339**, 811.

3 H. Yaghoobnejad Asl, K. Ghosh, M. P. Vidal Meza, A. Choudhury, *J. Mater. Chem. A*, 2015, **3**, 7488.

4 H. Yaghoobnejad Asl, A. Choudhury, *Inorg. Chem.*, 2015, **54**, 6566.

5 I. Munaò, E. A. Zvereva, O. S. Volkova, A. N. Vasiliev, A. R. Armstrong, P. Lightfoot, *Inorg. Chem.*, 2016, **55**, 2558.

6 H. Xing, W. Yang, T. Su, Y. Li, J. Xu, T. Nakano, J. Yu, R. Xu, *Angew. Chem. Int. Ed.*, 2010, **49**, 2328.

7 L. Zhao, J. Li, P. Chen, G. Li, J. Yu, R. Xu, *Chem. Mater.*, 2008, **20**, 17.

8 Z. Wang, K. Hu, S. Gao, H. Kobayashi, *Adv. Mater.*, 2010, **22**, 1526; E. Eikeland, N. Lock, M. Filsø, M. Stingaciu, Y. Shen, J. Overgaard, B. B. Iversen, *Inorg. Chem.*, 2014, **53**, 10178; L. C. Gómez-Aguirre, B. Pato-Doldán, J. Mira, S. Castro-García, M. A. Señarís-Rodríguez, M. Sánchez-Andújar, J. Singleton, V. S. Zapf, *J. Am. Chem. Soc.*, 2016, **138**, 1122.

9 W. Liu, H-H. Chen, X-X. Yang, J-T. Zhao, *Eur. J. Inorg. Chem.*, 2005, 946.

10 P. Román, J. M. Gutiérrez-Zorrilla, *Chem. Educ.*, 1985, **62**, 167.

11 W. Yingua, *J. Appl. Crystallogr.*, 1987, **20**, 258.

12 A. C. T. North, D. C. Philips, F. S. Mathews, *Acta Crystallogr.*, 1968, **A24**, 351.

13 *CrysAlisPro CCD* and *RED*, version 171.35.19; Oxford Diffraction, Ltd.: Oxford, U.K., 2011.

14 G. M. Sheldrick, *SHELXS 97: Program for the Solution of Crystal Structures*, University of Göttingen, Germany, 1977.

15 G. M. Sheldrick, *SHELXL 97: Program for the Refinement of Crystal Structures*, University of Göttingen, Germany, 1977.

16 L. J. Farrugia, *J. Appl. Crystallogr.*, 1999, **32**, 837.

17 P. v. d. Sluis, A. L. Spek, SQUEEZE, *Acta Crystallogr., Sect. A*, 1990, **46**, 194.

18 A. L. Spek, PLATON, A Multipurpose Crystallographic Tool, Utrecht University, Utrecht, The Netherlands, 2005.

19 E. Dowty, *ATOMS: A Computer Program for Displaying Atomic Structures*, Shape Software, 512 Hidden Valley Road, Kingsport, TN, 1993; K. Momma, F. Izumi, *J. Appl. Crystallogr.*, 2008, **41**, 653.

20 J. Rodriguez-Carvajal, *Phys. B*, 1993, **192**, 55.

21 T. T. D. Nguyen, L. Dimesso, G. Cherkashinin, J. C. Jaud, S. Lauterbach, R. Hausbrand, W. Jaegermann, *Ionics*, 2013, **19**, 1229.

22 V. V. Guliants, J. B. Benziger, S. Sundaresan, *J. Catal.*, 1995, **156**, 298.

23 J. Orive, R. Fernández de Luis, J. Rodríguez Fernández, E. Legarra, F. Plazaola, M. I. Arriortua, *CrystEngComm*, 2014, **16**, 6066.

24 V. A. Blatov, A. P. Shevchenko, D. M. Proserpio, *Cryst. Growth Des.*, 2014, **14(7)**, 3576.

25 I. D. Brown, D. Altermatt, *Acta Crystallogr.*, 1985, **B41(4)**, 244.

26 S. Álvarez, D. Avnir, M. Llunel, M. Pinsky, *New. J. Chem.*, 2002, **26**, 996; M. Llunel, D. Casanova, J. Cirera, J.M. Bofill, P. Alemany, S. Álvarez, M. Pinski, D. Yatumir, *SHAPE v1.1a: Program for Continuous Shape Measure Calculations of Polyhedral Xn and MLn Fragments*, 2003.

27 J. Loub, *Acta Crystallogr.*, 1991, **B47(4)**, 468.

28 U-C. Chung, J. L. Mesa, J. L. Pizarro, I. de Meatza, M. Bengoechea, J. Rodríguez Fernández, M. I. Arriortua, T. Rojo, *Chem. Mater.*, 2011, **23**, 4317.

29 E. S. Larrea, J. L. Mesa, E. Legarra, A. T. Aguayo, M. I. Arriortua, *Acta Crystallogr.*, 2016, **E72**, 63.

30 T. Berrocal, J. L. Mesa, E. Larrea, J. M. Arrieta, *Acta Cryst.*, 2014, **E70**, 309.

31 K. Nakamoto, *Infrared and Raman Spectroscopy of Inorganic and Coordination Compounds*. New York: John Wiley & Sons, 1997.
32 G. Kortum, *Reflectance Spectroscopy*, Springer, New York, 1969.
33 I. de Pedro, J. M. Rojo, J. Rius, O. Vallcorba, I. Ruiz de Larramendi, J. Rodríguez Fernández, L. Lezama, T. Rojo, *Inorg. Chem.*, 2012, **51**, 5246.
34 E. S. Larrea, J. L. Mesa, J. L. Pizarro, R. Fernández de Luis, J. Rodríguez Fernández, T. Rojo, M. I. Arriortua, *Dalton Trans.*, 2012, **41**, 14170.
35 B. F. Alfonso, C. Piqué, C. Trobajo, J. R. García, E. Kampert, U. Zeitler, J. Rodríguez Fernández, M. T. Fernández-Díaz, J. A. Blanco. *Physical Review B*, 2010, **82**, 144431.
36 B. F. Alfonso, C. Trobajo, C. Piqué, M. T. Fernández-Díaz, J. Rodríguez Fernández, M. A. Salvadó, P. Pertierra, S. García-Granda, J. R. García, J. A. Blanco. *Acta Materialia*, 2010, **58**, 1741.
37 D. P. Rojas, J. I. Espeso, J. Rodríguez Fernández, J. C. Gómez Sal, J. Sanchez Marcos, H. Müller, *Phys. Rev. B*, 2009, **80**, 184413.
38 V. K. Pecharsky, K. A. Gschneidner Jr., *J. Appl. Phys.*, 1999, **86**, 565.
39 R. Sessoli, *Angew. Chem. Int. Ed.*, 2012, **51**, 43.
40 L .C. Wang, Q. Y. Dong, J. Lu, X. P. Shao, Z. J. Mo, Z. Y. Xu, J. R. Sun, F. X. Hu, B. G. Shen, *J. Alloys Compd*., 2014, **587**, 10.
41 J. Sánchez Marcos, J. Rodríguez Fernández, B. Chevalier, *J. Magn. Magn. Mater*, 2007, **310**, 383.
42 I. A. Campbell, L. Bernardi, *Phys. Rev. B*, 1995, **52(14)**, R9819.

